

NRL Report 5981

UNCLASSIFIED

STOCHASTIC ESTIMATES OF THE PENETRATION OF GAMMA RAYS THROUGH SLAB SHIELDS

A. G. Pieper and L. A. Beach

Nuclear Reactions Branch
Radiation Division

September 26, 1963



U. S. NAVAL RESEARCH LABORATORY
Washington, D.C.

CONTENTS

| | |
|-------------------------------------|----|
| Abstract | ii |
| Problem Status | ii |
| Authorization | ii |
| INTRODUCTION | 1 |
| GAMMA-RAY TRANSPORT EQUATION | 1 |
| NAREC MACHINE PROGRAM | 4 |
| SELECTION OF BIASING FRACTION | 6 |
| COMPUTATIONAL RESULTS | 7 |
| COMPARISON OF COMPUTATIONAL RESULTS | 10 |
| Successive Scattering Method | 10 |
| Moment Method | 13 |
| ANALYSIS OF COMPUTATIONAL RESULTS | 20 |
| CONCLUSION | 31 |
| REFERENCES | 32 |

ABSTRACT

The energy penetration and dose-rate buildup factors have been calculated by Monte Carlo techniques on a digital computer for a plane, monodirectional source of gamma rays of 1.0, 2.5, and 6.0 Mev incident at various angles upon finite slab shields of lead, iron, ordinary concrete, and water. The exponential transformation and equivalent integration over the spatial variable were utilized to obtain results for slabs up to 18 mean-free-pathlengths in thickness. A simple expression was derived which relates a given buildup factor at any incident angle to the corresponding buildup factor at normal incidence.

PROBLEM STATUS

This is a final report on one phase of the problem; work on the problem is continuing.

AUTHORIZATION

NRL Problem HO1-10
Project RR 002-06-41-5006

Manuscript submitted June 13, 1963.

CONFIDENTIAL

STOCHASTIC ESTIMATES OF THE PENETRATION OF GAMMA RAYS THROUGH SLAB SHIELDS

INTRODUCTION

Early studies by Beach et al. (1) demonstrated that the exponential transformation (2) type of biasing was a useful technique when random sampling or Monte Carlo methods are used to solve deep gamma-ray penetration problems. It was shown by estimating the penetrations of 6-Mev photons through lead slabs that the exponential transformation was easier to apply and gave more accurate results than some other biasing techniques. As an additional check on the Monte Carlo technique using the exponential transformation, a solution (3) was obtained for the classic one-velocity neutron transport equation, which for certain source terms can be solved exactly. The Monte Carlo solution of the transformed transport equation was in excellent agreement with the exact solution for penetrations up to 20 mean-free-pathlengths. Therefore, it was decided to utilize the exponential transformation in a systematic Monte Carlo investigation of the energy penetration and dose-rate buildup factors for primary gamma ray energies of 1.0, 2.5, and 6.0 Mev. The photons were incident at angles from 0 to 55 degrees (measured from the normal to the material) in 11-degree increments and were directed upon finite slab shields of lead, iron, ordinary concrete, and water up to 18 mean-free-pathlengths in thickness.

GAMMA-RAY TRANSPORT EQUATION

In general the equations describing the transport of gamma rays or neutrons through a scattering medium cannot be solved analytically. The moment method (4), a powerful numerical technique normally requiring large amounts of computer time, has been very successfully applied to problems with various types of source geometries incident on an infinite homogenous media. However, in the case of finite media or other complicated geometries, random sampling or Monte Carlo techniques are much more suitable.

The Monte Carlo method arrives at an estimate to the solution of the transport equation by averaging over a large number of life histories. The life histories of gamma rays traversing from the source into or through the medium are generated by a random sampling or Monte Carlo process. By random sampling under the appropriate probability distributions for the various gamma-ray interactions, the transport history of this fictitious gamma ray is created step by step. The photons are normally not allowed to die through absorptive processes but are forced to scatter. The exclusion of the absorptive processes is compensated by weighting each gamma ray with a survival probability after each interaction. The survival probability after an interaction is equal to the ratio of the sum of nonabsorptive cross sections to the total cross section prior to the interaction; that is,

$$S_i = \frac{\overset{\text{Compton}}{\mu} (E_{i-1}) + \overset{\text{pair}}{\mu} (E_{i-1})}{\mu^t(E_{i-1})} \quad (1)$$

A gamma-ray history was terminated either when it reached the low energy cutoff or after it had undergone eight collisions.

Since the Monte Carlo method is statistical, its estimate to the solution of a particular transport problem can be improved by generating more histories. Statistical theory shows that the probable error is inversely proportional to the square root of the number of photons penetrating the shield. Therefore, a significant number of photons must penetrate the shield in order to obtain meaningful results. Doubling the number of photon histories will double the number of successful penetrations, but the probable error is only reduced by a factor of 0.707; therefore, in order to maintain the same probable error in the penetration probability as the shield thickness is increased, the number of incident photons must be increased exponentially because of the exponential attenuation of the shield. One method of reducing the number of photons required to obtain a certain probable error is to bias the gamma interaction probabilities so that the probability of penetration is increased. Many biasing techniques have been suggested, but most require the application of considerable physical intuition in order to obtain meaningful results. In contrast, the exponential transformation type of biasing is a natural and physically understandable means of biasing gamma-ray histories.

Some of the advantages of the exponential transformation can be illustrated by considering the transport equation and the resultant transformed transport equation of gamma rays traversing a laterally infinite slab shield. If $\psi(x, E, \theta)$ is the density of photons with energy E , a penetration distance x , and having a direction in an increment of solid angle about θ (the angle with the normal), then the transport equation governing ψ is

$$(\cos \theta) \frac{\partial \psi}{\partial x} + \mu(E) \psi = \int_{\theta'} \int_{E'} K(E, E', \theta, \theta') \psi dE' d\theta' + S(E, \theta) \delta(x) \quad (2)$$

where $\mu(E)$ is the total absorption coefficient, the integral represents the usual scattering term, and $S(E, \theta) \delta(x)$ is the source term which involves a delta function. If the substitution

$$\psi = \bar{\psi} e^{-cx} \quad (3)$$

is made, the transport equation becomes

$$\begin{aligned} & (\cos \theta) \frac{\partial \bar{\psi}}{\partial x} + [\mu(E) - c \cos \theta] \bar{\psi} \\ & = \int_{\theta'} \int_{E'} K(E, E', \theta, \theta') \bar{\psi} dE' d\theta' + S(E, \theta) \delta(x) \end{aligned} \quad (4)$$

where the source term is unchanged because $e^{cx} \delta x$ is equivalent to $\delta(x)$.

This transformed transport equation for $\bar{\psi}$ is the same form as the original equation in terms of a modified absorption coefficient $\bar{\mu}(E)$ defined as

$$\bar{\mu}(E) = \mu(E) - c \cos \theta. \quad (5)$$

Thus photons undergo the same scattering processes as before the transformation, but now the absorption coefficient has been reduced, especially in the forward direction, $\theta = 0^\circ$. This is just the type of biasing that is required for deep penetration problems, because in the physical media, only those photons headed in the forward direction can have any significant probability of penetrating the media, and these are the photons which must be given greater emphasis.

It can be seen from Eq. (5) that the transformation constant c must have the dimensions of an absorption coefficient and in fact can be equated to some fraction of the total absorption

coefficient at the incident energy; that is,

$$c = F \mu(E_0) \quad (6)$$

with the condition that the biasing fraction F must be within the limits

$$0 < F < \frac{\mu_{(\min)}(E)}{\mu(E_0)} \quad (7)$$

where $\mu(E_0)$ is the absorption coefficient of the shielding material at the energy of the incident photon, and $\mu_{(\min)}(E)$ is the minimum value of the absorption coefficient of the shield material at an energy equal to or less than the energy of the incident photon.

The effectiveness of the exponential transformation type of biasing can be seen by substituting Eq. (6) into Eq. (3) and transposing

$$\bar{\psi} = \psi e^{+F \mu(E_0)x} \quad (8)$$

This equation shows that the attenuation of the transformed shield has been reduced by the exponential factor, i.e., the density of photons has been increased. This is an enormous reduction factor for thick shields even if the biasing fraction is conservatively chosen as 0.5. The reduction in the number of photon histories required to estimate $\bar{\psi}$ is thereby decreased by approximately this same factor. The maximum value of the biasing fraction will minimize the number of photon histories, but the resultant expression for ψ is a very poor approximation for a thick shield. The effect on ψ can best be illustrated by setting the biasing fraction equal to 1.0 for the case of normally incident photons. Under these conditions, it can be shown from Eq. (5) and (6) that the modified absorption coefficient will be zero. This means that no photon interactions are possible, and therefore $\bar{\psi}$ will be equal to 1.0. Consequently from Eq. (8) we find that the estimated penetration probability is

$$\psi = e^{-\mu(E_0)x} \quad (9)$$

but this is just equal to the uncollided penetration probability of primary photons through a slab x centimeters thick. Thus, in effect, a biasing fraction of 1.0 will completely eliminate any contribution to the total penetration probability from any scattered photons. It is the scattered photon contribution that is the dominant part of the total penetration probability for thick shields. Therefore, the biasing fraction must be somewhat less than 1.0 so that an estimation of the scattered contribution is possible, using a reasonable number of photon histories.

It was found that 10,000 gamma histories could be calculated in less than an hour, so this number of photon histories was used in all calculations. It seemed very likely that an optimum biasing fraction exists if a given number of photon histories are used; thus a study of the effect of varying the biasing fraction was made and will be described subsequently.

Further improvement of the Monte Carlo estimates is possible by use of the "expected value" technique. If any part of the problem can be solved analytically, this is done instead of using the random sampling. For example, instead of counting the number of photons which cross a boundary, it is much more economical to calculate the probability of crossing that boundary after every nondestructive photon interaction.

The technique of prohibiting an absorption interaction was used in solving the transformed transport equation. The survival probability, Eq. (1), must be modified by using

the modified total cross section $\bar{\mu}^t(E)$ in place of the total cross section $\mu^t(E)$. The modified survival probability is therefore

$$\bar{S}_i = \frac{\overset{\text{Compton pair}}{\mu(E_{i-1})} + \mu(E_{i-1})}{\bar{\mu}^t(E_{i-1})} \quad (10)$$

NAREC MACHINE PROGRAM

A program was coded for NAREC (Naval Research Electronic Computer) which solved the exponentially transformed transport equation by the Monte Carlo method. The transport equation was solved for the case of a plane-parallel, monoenergetic, monodirectional source of gamma rays incident upon finite slabs of various shielding materials at fixed angles.

The program generated gamma-ray histories in the usual manner. After every gamma interaction, which is either scattered (Compton process) or reradiated (pair process) in the forward direction, the probability of penetrating the slab shield was calculated. This probability was weighted by the energy of the photon as well as its survival probability, and the resultant, called the energy penetration probability, was recorded in an energy interval appropriate to the energy of the photon. Whenever a pair process occurred, only one of the annihilation quanta were followed, but its weight was doubled.

Dose-rate probability due to each of the penetrating photons was calculated and tabulated. The dose-rate probability is equal to the energy flux penetration probability times the energy absorption coefficient in air in cm²/gram. The energy flux penetration is equal to the energy penetration times the reciprocal of the cosine of the angle that the photon emerges from the shield.

Instead of calculating the penetration probability of a single thickness shield during each run on the computer, the penetration probabilities for six different shield thicknesses were calculated. This was accomplished by visualizing the shield as infinite with barriers positioned parallel to the front face of the shield at multiples of the mean-free-pathlength of the incident radiation. These barriers were made to represent a slab shield of corresponding thickness by prohibiting a contribution to the forward penetration probability at a barrier once the photon has crossed that barrier. The barriers were placed three mean-free-pathlengths apart for the majority of the runs.

The photon histories were followed until they penetrated either the front (reflection) or rear (transmission) faces of the shield or they reached either the low energy or maximum number of collision cutoffs. The low energy cutoff must be selected so that the expected contribution from the photons below this energy is small compared to the total penetration probability. The low energy cutoff is therefore a function of the incident energy. The maximum number of collisions allowed was conservatively chosen as eight.

The energy penetration probability was tabulated in energy intervals which were 0.125 Mev wide in the energy range from 0.25 to 1.0 Mev; 0.25 Mev wide from 1.0 to 2.5 Mev and 0.50 Mev wide from 2.5 to 7.0 Mev. The incident energy was restricted to less than 7.0 Mev because the program only allowed three processes to occur, i.e., Compton, pair, and photoelectric. Secondary processes, such as bremsstrahlung, can become important at higher energies.

A table of the values of the various absorption coefficients (total, Compton, and pair, as well as the energy absorption coefficient for air) was coded for each of the shielding materials. The energy for which the coefficients were tabulated corresponded to the mean

energy in each of the energy intervals that were used for the transmitted energy and dose spectra. The absorption coefficients for lead, iron, and water were obtained from the compilation by G. White Grodstein (5). The coefficients for ordinary concrete having a density of 2.3 g/cm³ and the composition given in Table 1 were computed by Dr. C. M. Davisson (6).

Table 1
Composition of Ordinary Concrete
(Density = 2.3 g/cm³)

| Element | Percent By Weight |
|---------|----------------------|
| H | 1.0 |
| O | 52.9 |
| Si | 33.7 |
| Al | 3.4 |
| Ca | 4.4 |
| Fe | 1.4 |
| Mg | 0.2 |
| NA | 1.6 |
| K | 1.3 |
| C | 0.1 |
| Total | 100.0 |

For each set of initial parameters, such as shield material, incident energy, and angle of primary photons, 10,000 gamma histories were generated. The program actually divided each run into 10 subgroups of 1,000 histories each, so that an assessment of the statistical fluctuation in the data could be made.

After every 1,000 histories, the energy penetration and dose-rate buildup factors were calculated and stored. The energy penetration buildup factor is defined, for a given set of conditions, such as the energy and configuration of the gamma-ray source, as being equal to the sum of the energy penetration probabilities of those photons which have undergone exactly none, one, two, etc., collisions before emerging from the shield normalized by the uncollided energy penetration probability of an equivalent number of primary photons at normal incidence. The energy penetration buildup factor can be written as

$$B_T(M, E_0, \theta_0, \tau_0) = \frac{\sum_{k=0}^{\infty} \mathcal{E}_k(M, E_0, \theta_0, \tau_0)}{\mathcal{E}_0(M, E_0, 0^\circ, \tau_0)} \quad (11)$$

where \mathcal{E}_k is the energy penetration probability of photons that undergo exactly k scatterings before penetrating the shield. The subscript T on the buildup factor denotes energy transmission or energy penetration because E is commonly used to designate energy flux. Dose-rate buildup factors are defined similarly. The subscript R is used to designate dose-rate. The conditions for which a particular buildup factor is defined are designated by M, the material of the shield; E_0 , the energy of incident photon; θ_0 , the incident angle of the photon; and τ_0 [$\tau_0 = \mu(E_0) x$], the thickness of the shield in mean-free-pathlengths of incident radiation. Actually the configuration of the source and the shielding medium must also be

specified, but for this calculation, these parameters were fixed. That is, the source is a plane-parallel monodirectional source, and the medium is a laterally infinite slab shield.

Buildup factors are rather cumbersome parameters, but they are useful in practical shielding applications. The usefulness of the various kinds of buildup factors is more apparent if Eq. (11) is written in the following form:

$$\sum_{k=0}^{\infty} \mathcal{E}_k(M, E_0, \theta_0, \tau_0) = B_T(M, E_0, \theta_0, \tau_0) \mathcal{E}_0(M, E_0, 0^\circ, \tau_0). \quad (12)$$

That is, the summation on the left which is required in shieldings applications can be replaced by the product of the appropriate buildup factor and the uncollided energy penetration probability at normal incidence, which is simply

$$\mathcal{E}_0(M, E_0, 0^\circ, \tau_0) = E_0 e^{-\tau_0}. \quad (13)$$

The total time on NAREC for each run was predominately a function of the low energy cutoff and to a lesser degree a function of the incident photon energy and shield material. For the higher incident energies and heavier materials, a low energy cutoff of 0.375 Mev was used, whereas 0.25 Mev was used at lower energies. With these cutoff energies, the computing time for 10,000 histories did not exceed 60 minutes, with about 20 percent of this time required by the slow output section of NAREC.

SELECTION OF BIASING FRACTION

In order to determine whether there was an optimum biasing fraction, a specific shielding problem was computed with a sequence of different biases. Six differently biased, gamma-ray transmission runs, each run consisting of 10,000 photon histories, were made using 6.0-Mev photons at normal incidence upon lead slab shields up to 18 mean-free-path-lengths thick. The energy penetration buildup factor appeared to be the most amenable criteria for selecting an optimum bias factor since measurements of gamma-ray transmission through very thick shields are not available for this purpose. The energy penetration buildup factors are plotted as a function of the biasing fraction F in Fig. 1 for slab shields 3 to 18 mean-free-pathlengths thick. Since there is a minimum in the absorption coefficient for lead below this energy ($E_0 = 6.0$ Mev), the transformation constant c (Eq. 6) was equated to a fraction of the minimum absorption coefficient for lead, i.e., $c = F\mu_{\min}$.

It can be seen in Fig. 1, that overbiasing can result in an underestimation of the buildup factor especially as the shield thickness increases. This fall-off of the energy penetration buildup factor is caused by the excessive reduction of the probability of not only the singly scattered photons, but also of the doubly, triply, etc., scattered photons as the effective thickness of the transformed shield is reduced. In actuality, the contribution from the scattered photons is the major penetration component for thick shields as is evident from the magnitude of the buildup factor for thick shields. When these results are considered in the light of the kind of accuracy required in practical shielding applications, the selection of the biasing fraction is not too critical for these conditions. The data in Fig. 1 indicate that a value of approximately 0.70 would be a reasonable compromise for the biasing fraction. However, since gamma-ray transmission through slab shields at oblique angles of incidence was contemplated, the biasing fraction was made a function of the incident angle. A relationship was desired that would increase the bias as the incident angle increased, so that the reduction of the slant penetration probability of the primary photons would be at least partially compensated. The relationship chosen was

$$F = \cos \frac{1}{4} (180^\circ - \theta_0) \quad (14)$$

Fig. 1 - Estimates of the energy penetration buildup factors, $B_T(\text{Pb}, 6.0, 0^\circ, \tau_0)$, as a function of biasing fraction F for various slab thicknesses (τ_0) where τ_0 is expressed in mean-free-paths (mfp)

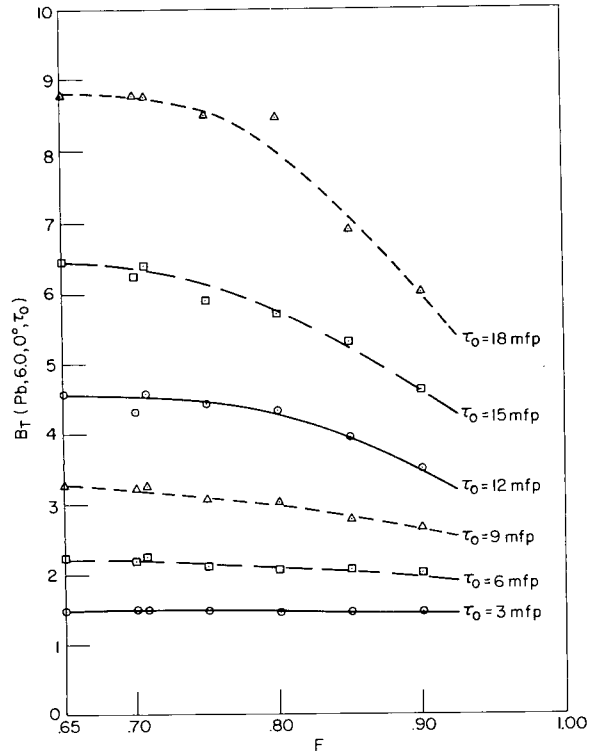


Table 2
Values of Biasing Fraction F as a
Function of Incident Angle

| θ_0 (degrees) | F |
|----------------------|-------|
| 0 | 0.707 |
| 11 | 0.740 |
| 22 | 0.771 |
| 33 | 0.801 |
| 44 | 0.829 |
| 55 | 0.855 |

This function gives a biasing fraction of 0.707 for normal incident photons, which is in the region in Fig. 1 where the buildup factors have essentially reached their maximum value. In Table 2 are values of this function for a number of incident angles.

Since the selection of the biasing fraction for this particular energy and material was not critical, it was decided to use this biasing fraction formula for all succeeding calculations. Whether the bias does in fact generate realistic estimates of the buildup factors cannot be ascertained from the data itself. Subsequent comparison of our results, using this formula for various shielding materials with the results of other investigators, indicates that this formula for the biasing fraction is quite good.

COMPUTATIONAL RESULTS

A summary of the energy penetration and dose-rate buildup factors for a plane, mono-directional source of gamma rays is plotted in Figs. 2-9. The energy penetration and dose-rate buildup factors for lead, iron, ordinary concrete, and water are plotted as a function of slab thickness in mean-free-pathlengths of the primary radiation for normally incident photons of 1.6, 2.5, and 6.0 Mev energy.

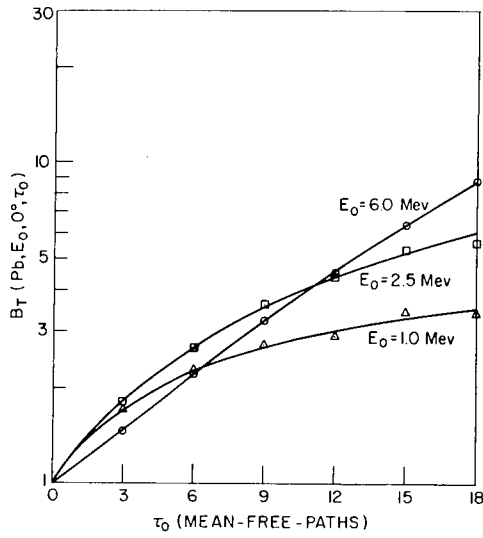


Fig. 2 - Energy penetration buildup factors, $B_T(\text{Pb}, 6.0, 0^\circ, \tau_0)$, $B_T(\text{Pb}, 2.5, 0^\circ, \tau_0)$, and $B_T(\text{Pb}, 1.0, 0^\circ, \tau_0)$ as a function of slab thickness τ_0

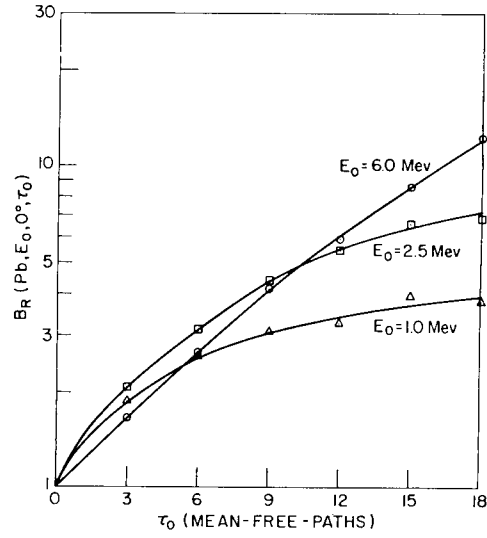


Fig. 3 - Dose-rate buildup factors, $B_R(\text{Pb}, 6.0, 0^\circ, \tau_0)$, $B_R(\text{Pb}, 2.5, 0^\circ, \tau_0)$, and $B_R(\text{Pb}, 1.0, 0^\circ, \tau_0)$, as a function of slab thickness τ_0

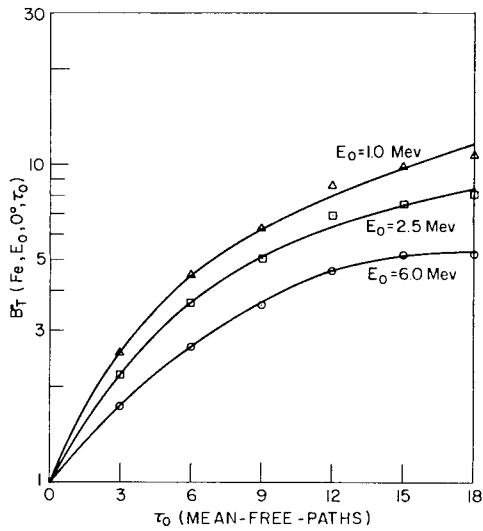


Fig. 4 - Energy penetration buildup factors, $B_T(\text{Fe}, 6.0, 0^\circ, \tau_0)$, $B_T(\text{Fe}, 2.5, 0^\circ, \tau_0)$, and $B_T(\text{Fe}, 1.0, 0^\circ, \tau_0)$ as a function of slab thickness τ_0

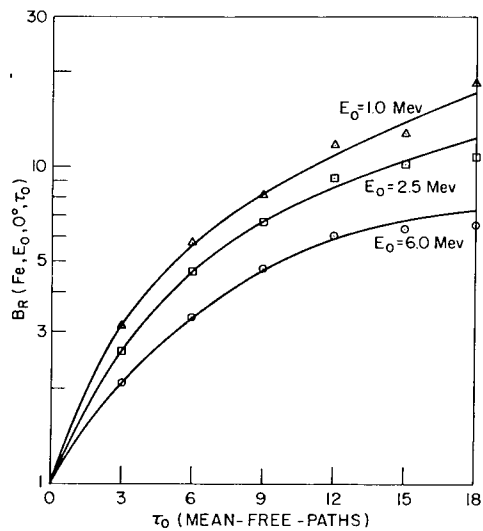


Fig. 5 - Dose-rate buildup factors, $B_R(\text{Fe}, 6.0, 0^\circ, \tau_0)$, $B_R(\text{Fe}, 2.5, 0^\circ, \tau_0)$, and $B_R(\text{Fe}, 1.0, 0^\circ, \tau_0)$ as a function of slab thickness τ_0

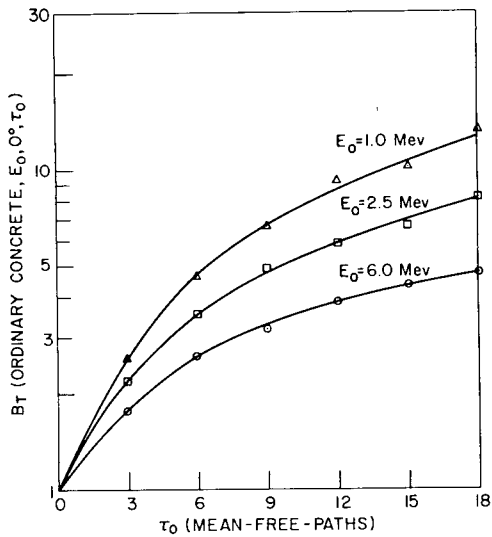


Fig. 6 - Energy penetration buildup factors B_T (concrete, 6.0, $0^\circ, \tau_0$), B_T (concrete, 2.5, $0^\circ, \tau_0$) and B_T (concrete, 1.0, $0^\circ, \tau_0$) as a function of slab thickness τ_0

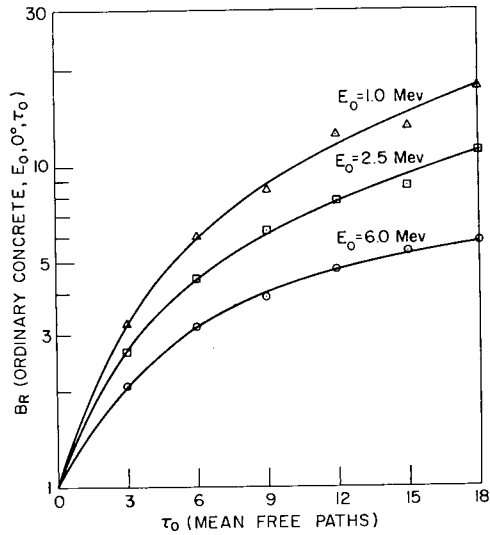


Fig. 7 - Dose-rate buildup factors, B_R (concrete, 6.0, $0^\circ, \tau_0$), B_T (concrete, 2.5, $0^\circ, \tau_0$) and B_R (concrete, 1.0, $0^\circ, \tau_0$), as a function of slab thickness τ_0

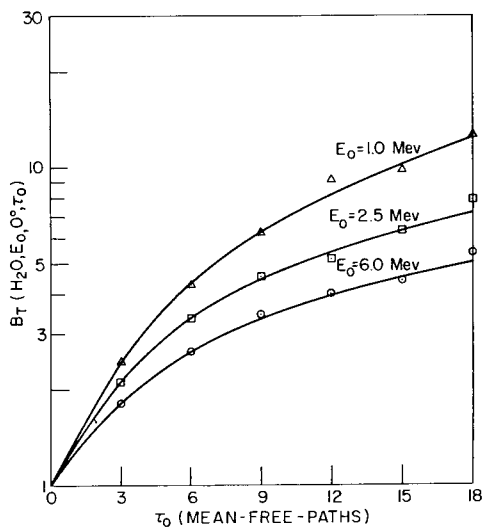


Fig. 8 - Energy penetration buildup factors, $B_T(H_2O, 6.0, 0^\circ, \tau_0)$, $B_T(H_2O, 2.5, 0^\circ, \tau_0)$ and $B_T(H_2O, 1.0, 0^\circ, \tau_0)$, as a function of slab thickness τ_0

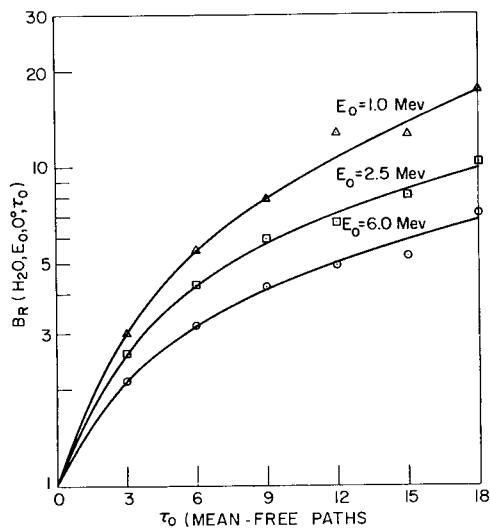


Fig. 9 - Dose-rate buildup factors, $B_R(H_2O, 6.0, 0^\circ, \tau_0)$, $B_R(H_2O, 2.5, 0^\circ, \tau_0)$ and $B_R(H_2O, 1.0, 0^\circ, \tau_0)$, as a function of slab thickness τ_0

The energy penetration and dose-rate buildup factors of gamma rays at other than normal incidence are not included here because an analysis of these buildup factors has produced a simple expression relating these buildup factors to the corresponding buildup factors of gamma rays at normal incidence. This expression is derived and its limitations are discussed in the section on Analysis of Computational Results. This relationship can be written

$$B_x(M, E_0, \theta_0, \tau_0) = B_x(M, E_0, 0^\circ, \tau_0) e^{-[\sec(\beta_x \theta_0) - 1] \tau_0} \quad (15)$$

where $B_x(M, E_0, \theta_0, \tau_0)$ is the buildup factor of the quantity x when gamma rays of energy E_0 are incident at an angle θ_0 degrees upon a slab shielding material M of τ_0 mean-free-pathlength thickness. $B_x(M, E_0, 0^\circ, \tau_0)$ is the corresponding buildup factor of normally incident photons.

This equation permits the transformation of a buildup factor for normally incident photons into corresponding buildup factor for obliquely incident photons, provided the parameter β_x is known. Actually it has been found that β_x is between 0.80 and 0.95 for the materials and in the energy range investigated to date. The value of the parameter β for various shielding materials and energies is given in the section entitled Analysis of Computational Results.

COMPARISON OF COMPUTATIONAL RESULTS

Successive Scattering Method

The solution of the transport equation by the method of successive scatterings consists of calculating the expected energy of a photon transmitted through a slab with exactly k of scatterings. This method was used by Peebles (7) to obtain the transmission or penetration probability through finite slabs of iron and lead. It was possible to calculate these same probabilities with our program by varying the collisions per photon history cutoff. That is, a special problem was run allowing only one collision, then two collisions, etc. The contribution of each collision could then be determined. The results of these calculations for three different sets of parameters are shown in Figs. 10-12, along with those from the calculations of Peebles for similar conditions. The energy penetration probability of singly ($k = 1$), doubly ($k = 2$), and triply ($k = 3$) scattered photons, all being normalized by the uncollided energy penetration probability, is plotted as a function of slab thickness in mean-free-pathlengths. The agreement between the two methods is quite good except for the second scattering penetration probability of 6.0-Mev photons in lead.

Peebles only calculated probabilities out to the third collision and extrapolated to obtain probabilities for high collision numbers. He was thus able to arrive at energy penetration buildup factors by summing the various order scattering probabilities. The energy penetration buildup factors calculated by Peebles are indicated by the solid curves in Figs. 13 and 14. The data shown in Fig. 13 is for the case of 1.25-, 2.5-, and 5.0-Mev gamma rays normally incident on lead slabs, whereas the data in Fig. 14 is for corresponding gamma rays on iron slabs. Our energy penetration buildup factors for gamma rays of 1.0, 2.5, and 6.0 Mev energy are indicated by triangles, squares, and circles respectively. The agreement between our data and Peebles' data is quite good except for the 1.0- and 1.25-Mev gamma rays incident on lead, for which a greater difference exists between the curve and our data points than can be accounted for by the energy difference. It will be shown that our results are in closer agreement with the calculations of Goldstein at this energy. Our results for 6.0-Mev gammas on iron slabs appears to be an underestimation, and a subsequent run with a higher bias factor raised our values. Peebles computed the energy penetration buildup factors for several incident angles, but the comparison of this data will be reserved for the section on analysis of results. It can be stated here that the agreement is very good.

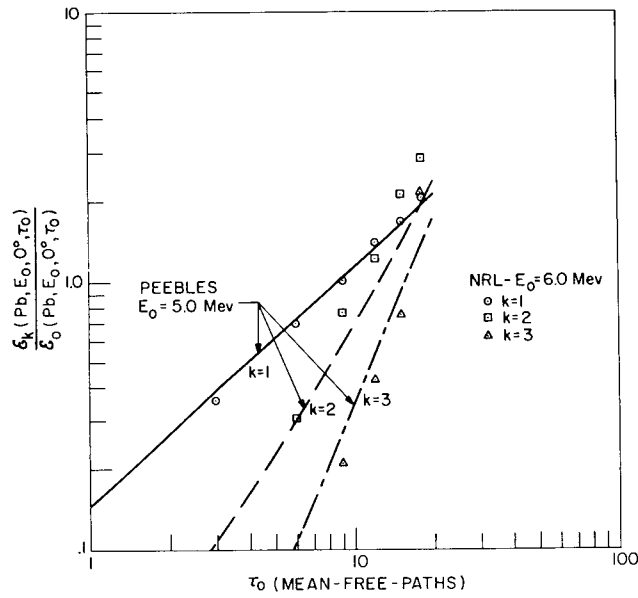


Fig. 10 - The ratio of the energy penetration probabilities of a photon which has encountered exactly k scatterings to that of an uncollided photon as a function of slab thickness τ_0 . Medium - lead; energy-5.0 and 6.0 Mev.

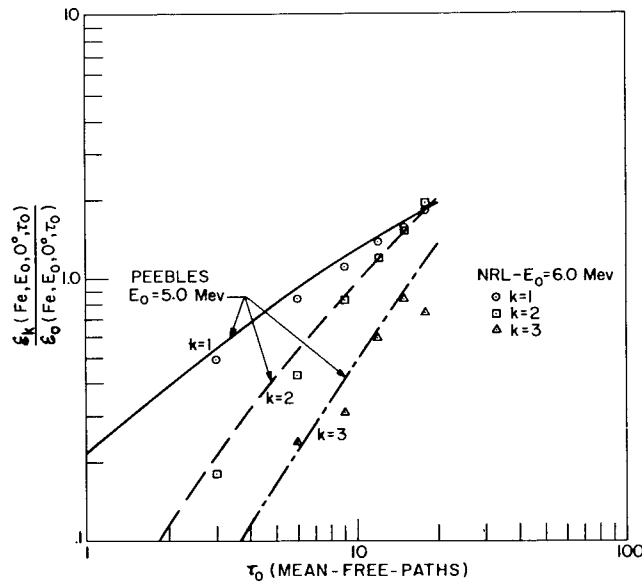


Fig. 11 - The ratio of the energy penetration probabilities of a photon which has encountered exactly k scatterings to that of an uncollided photon as a function of slab thickness τ_0 . Medium - iron; energy - 6.0 Mev.

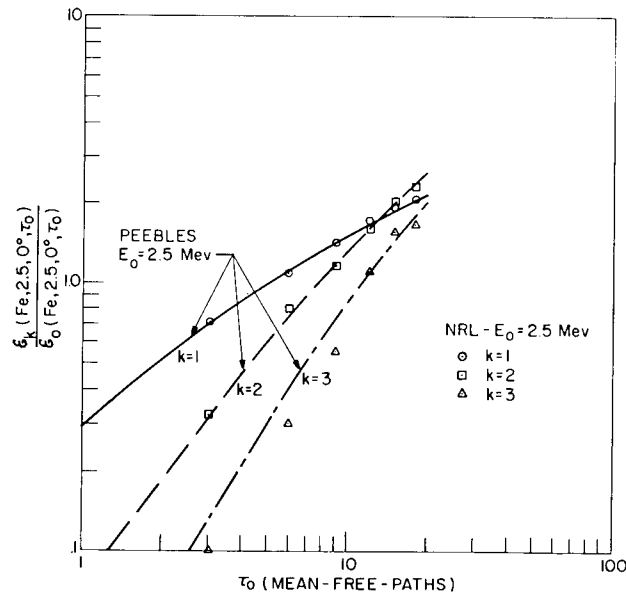


Fig. 12 - The ratio of the energy penetration probabilities of a photon which has encountered exactly k scatterings to that of an uncollided photon as a function of slab thickness τ_0 . Medium - iron; energy - 2.5 Mev.

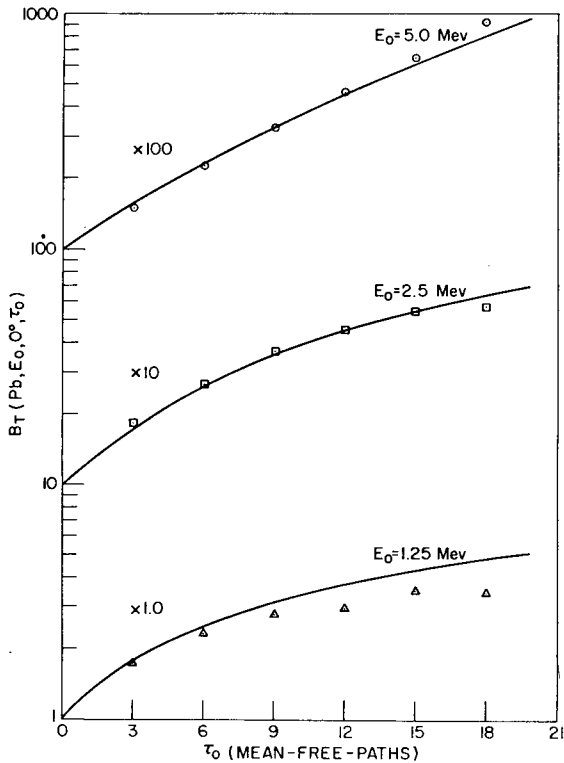


Fig. 13 - Comparison of Peebles (solid curves) and NRL (inscribed points) energy penetration buildup factors for three different gamma-ray energies in lead

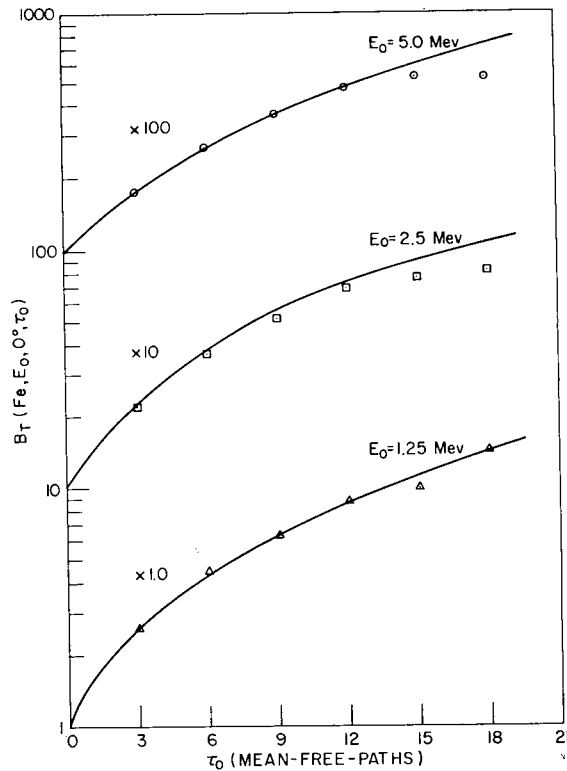


Fig. 14 - Comparison of Peebles (solid curves) and NRL (inscribed points) energy penetration buildup factors for three different gamma-ray energies in iron

Moment Method

The classic work in gamma attenuation was done by Goldstein (8) using the moment method. He has calculated the energy flux and dose-rate buildup factors as well as energy spectra for a wide range of incident energies and for numerous materials. His results apply to an infinite medium, but Berger and Doggett (9) have shown that the ratio of the buildup factor for finite medium to that for infinite material is greater than 0.90 at penetration distances greater than 8.0 mean-free-pathlengths and for energies greater than 1.0 Mev in the higher atomic number materials. Therefore, a comparison of results for the two different geometries should be appropriate. Since our program calculated the energy penetration rather than the energy flux, a direct comparison of this data was not possible. But it was possible to derive the energy flux from our dose-rate spectra, since dose-rate is proportional to flux. The dose-rate buildup factors were directly comparable, but a comparison of the energy flux spectra was also desired.

A comparison of our derived energy flux buildup factors and those of Goldstein's for photons of 1.0, 2.5, and 6.0 Mev, normally incident on lead, iron, and water can be seen in Figs. 15-17. The solid curves are Goldstein's data, and the inscribed points are our data. Goldstein's 2.5-Mev data was an interpolation of his data at 2.0 and 3.0 Mev. The agreement between our data and Goldstein's data is quite good out to 12 or 15 mean-free-pathlengths in lead and iron. The difference between our 1.0-Mev iron and water as well as our 2.5-Mev water data and that of Goldstein's is actually due to the difference in media configuration. This can be seen in the next series of curves in Figs. 18-26. These curves are the differential energy flux spectra for slab thicknesses of 3, 9, and 15 mean-free-pathlengths for the same energies and materials as before. The histograms are our energy

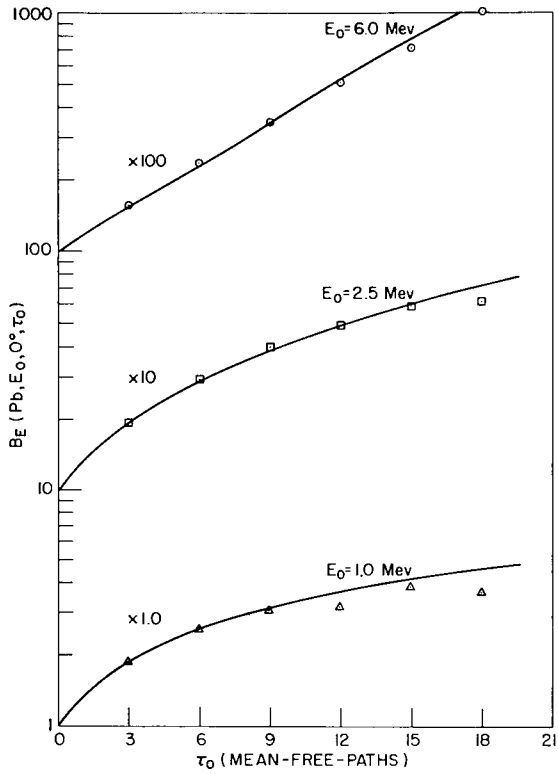
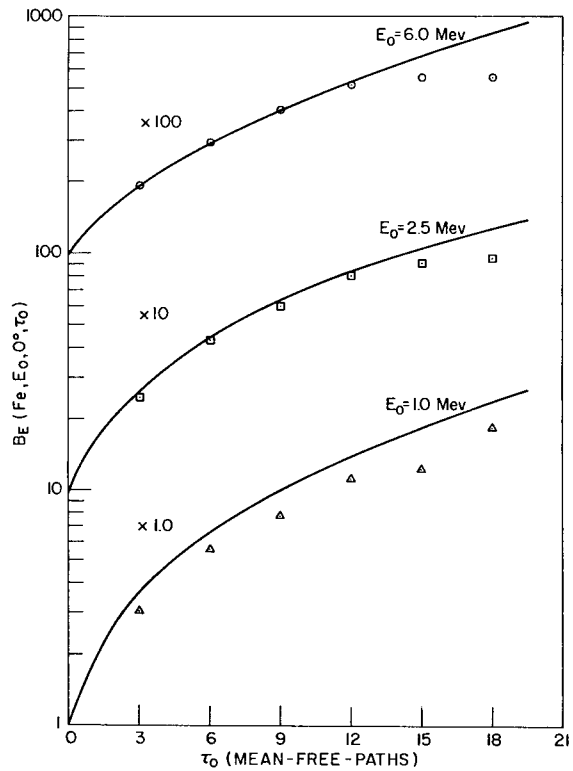


Fig. 15 - Comparison of Goldstein (solid curves) and NRL (inscribed points) energy flux buildup factors for three different gamma-ray energies in lead

Fig. 16 - Comparison of Goldstein (solid curves) and NRL (inscribed points) energy flux buildup factors for three different gamma-ray energies in iron



UNCLASSIFIED

Fig. 17 - Comparison of Goldstein (solid curves) and NRL (inscribed points) energy flux buildup factors for three different gamma-ray energies in water

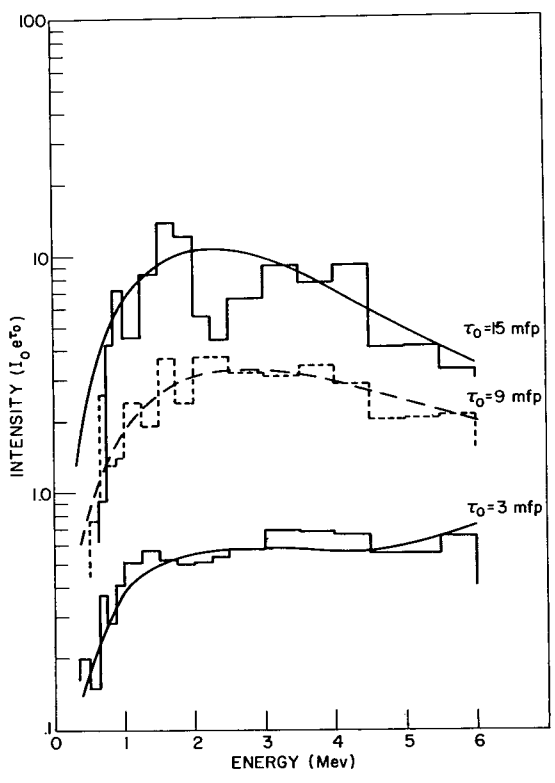
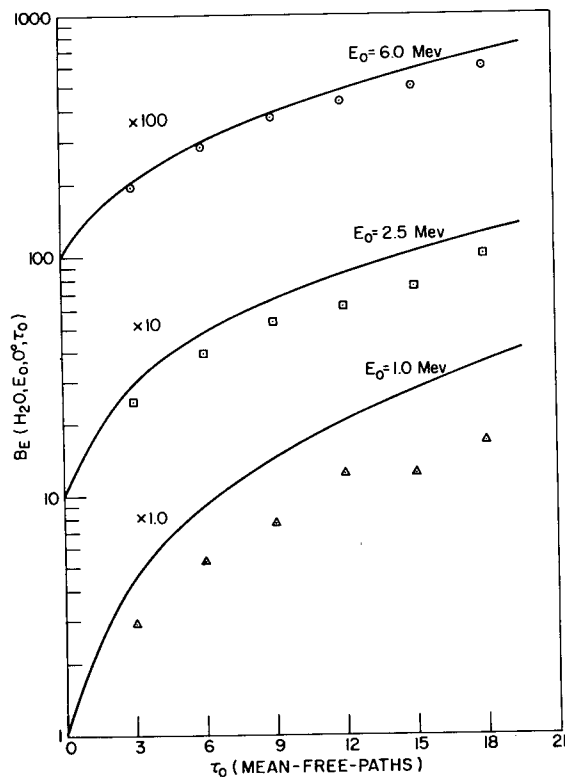


Fig. 18 - Differential energy flux spectrum. Medium - lead; energy - 6.0 Mev.

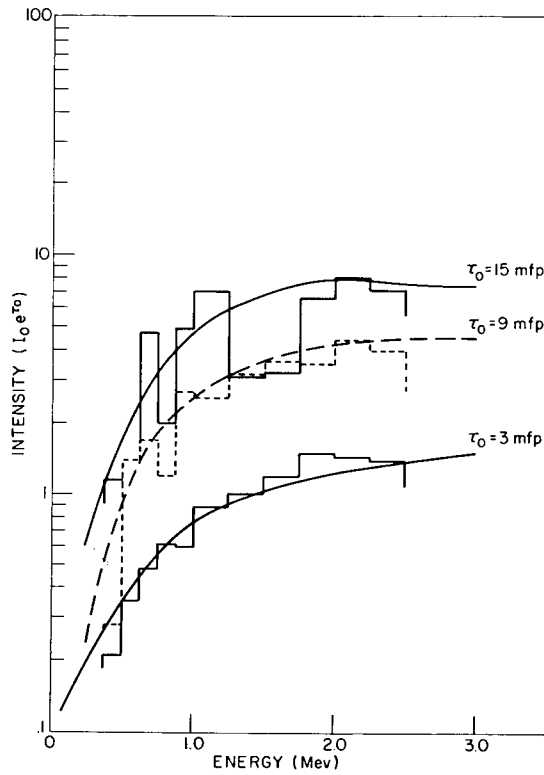


Fig. 19 - Differential energy flux spectrum. Medium - lead; energy - 2.5 and 3.0 Mev.

Fig. 20 - Differential energy flux spectrum. Medium - lead; energy - 1.0 Mev.

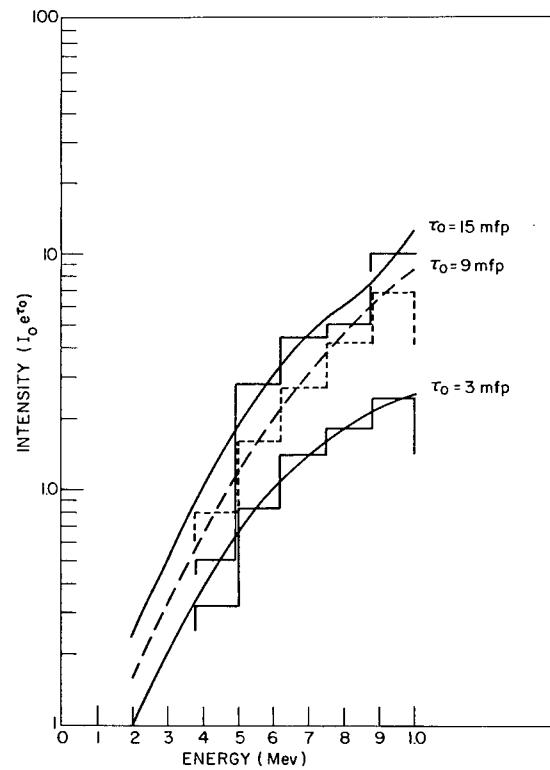


Fig. 21 - Differential energy flux spectrum. Medium - iron; energy - 6.0 Mev.

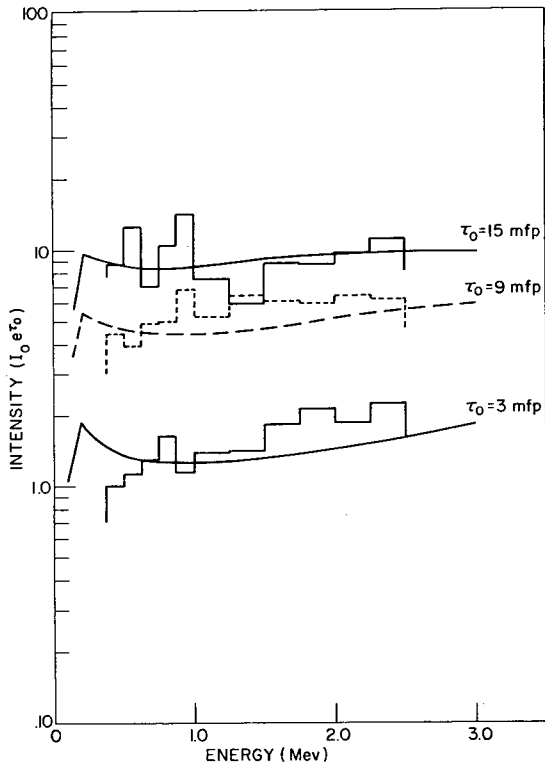
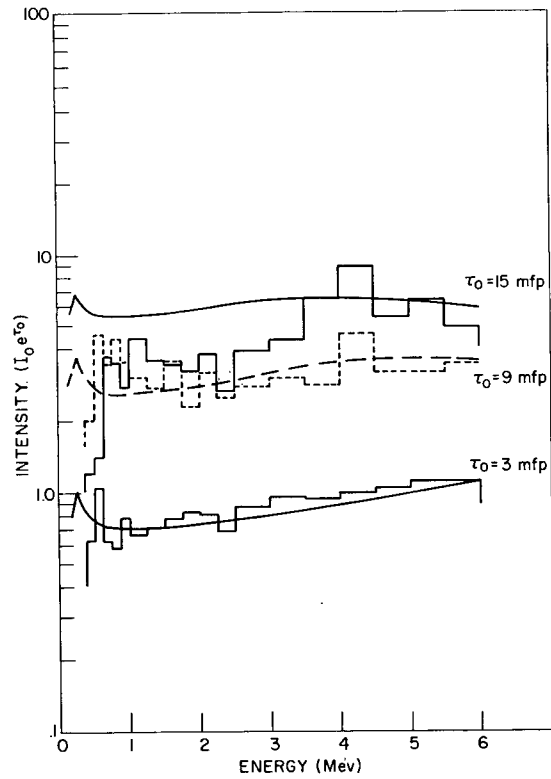


Fig. 22 - Differential energy flux spectrum. Medium - iron; energy - 2.5 and 3.0 Mev.

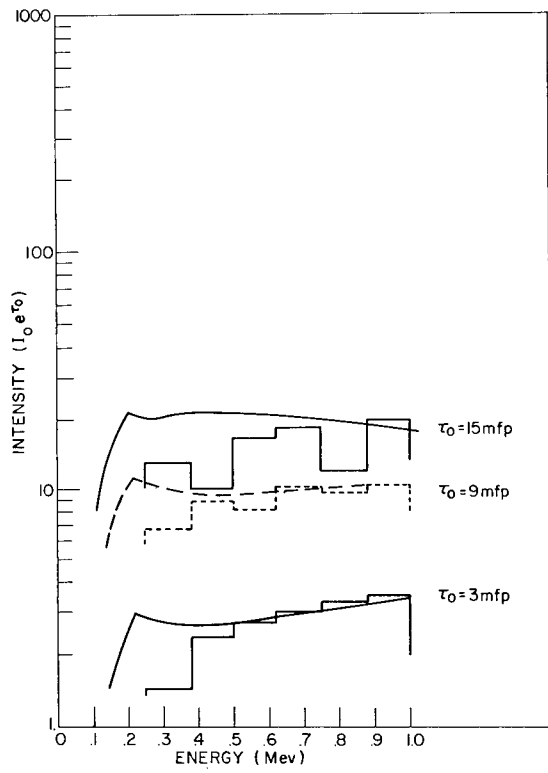


Fig. 23 - Differential energy flux spectrum. Medium - iron; energy - 1.0 Mev.

Fig. 24 - Differential energy flux spectrum. Medium - water; energy - 6.0 Mev.

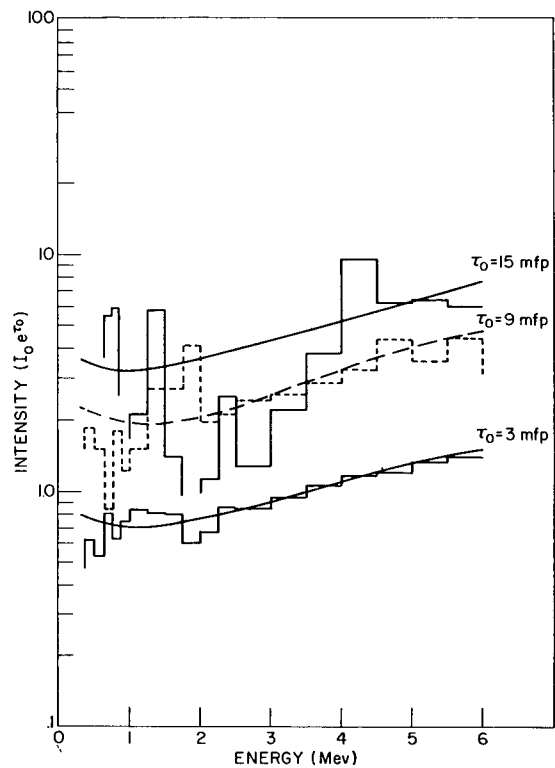


Fig. 25 - Differential energy flux spectrum. Medium - water; energy - 2.5 and 3.0.

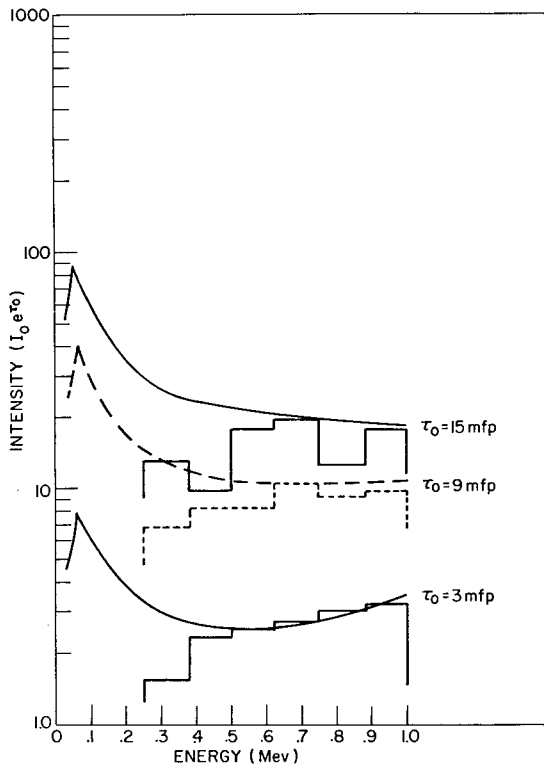
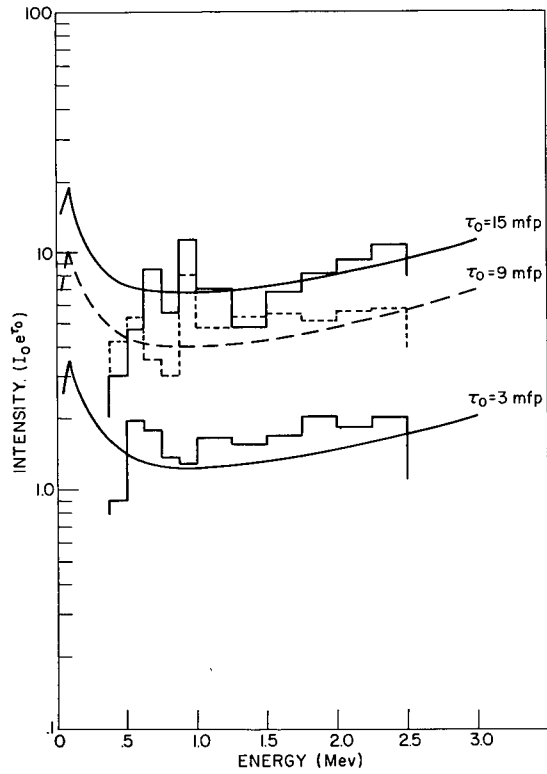


Fig. 26 - Differential energy flux spectrum. Medium - water; energy - 1.0 Mev.

spectra, whereas the smoothed curves are Goldstein's spectra. Our 2.5-Mev data is actually being compared to Goldstein's 3.0-Mev data because an interpolation of Goldstein's energy spectra was not attempted.

The agreement in the energy flux spectra for the 1.0-, 2.5-, and 6.0-Mev photons on lead is excellent, as is also the case for the lead buildup factors at these energies. The difference between the finite and infinite media is not discernible, because the high photoelectric absorption in lead at the low energies is eliminating any low energy component. It is only in the low energy region, that is, less than 0.50 Mev, that the infinite medium can have a higher differential energy spectra than the finite medium. This can be seen if one considers the infinite medium as being the same as the finite medium or slab with a contribution, i.e., a reflection, from a subsequent infinite slab. It has been shown by albedo calculations (10, 11) that if the incident photons are not near grazing incidence, then the reflected photons will have an energy less than 0.5 Mev, irrespective of the energy of the incidence photon. The albedo calculations have shown that the reflection from lead is practically zero, and thus the energy penetration for the finite and infinite media should be the same. However, there is appreciable albedo from iron and water, and therefore the energy penetration for these materials does depend on the media configuration. This can be seen especially for 1.0-Mev photons in iron or water. The finite media spectrum is falling off much faster than that for the infinite medium. This difference is sufficient to account for the differences in the 1.0-Mev energy flux buildup factor curves in Figs. 16 and 17. Our differential energy spectra at 15 mean-free-pathlengths for 6.0-Mev photons in both iron and water show significant departure from Goldstein's data. A rerun of our program, using a biasing fraction of 0.80 instead of 0.707 for 6.0-Mev photons on iron, increased the iron buildup factors from 5.5 to 6.3 at a penetration distance of 15 mean-free-pathlengths and from 5.5 to 7.10 at 18 mean-free-pathlengths, both of these values are slightly below Goldstein's data. Thus, it appears that the formula for the biasing fraction F (Eq. 14) is not too satisfactory for very thick iron shields.

ANALYSIS OF COMPUTATIONAL RESULTS

When the buildup factors were plotted as a function of slab thickness for various incident angles, it appeared that these curves were simply related. An example of these curves can be seen in Fig. 27, where the energy penetration buildup factors for 2.5-Mev gamma rays incident at various angles on iron slabs are plotted as a function of slab thickness in mean-free-pathlengths. This relationship was found by normalizing the buildup factors of obliquely incident gamma rays by the corresponding buildup factors of normally incident gamma rays and plotting the logarithm of this ratio as a function of slab thickness. This ratio is defined as

$$R_T(M, E_0, \theta_0, \tau_0) = \frac{B_T(M, E_0, \theta_0, \tau_0)}{B_T(M, E_0, 0^\circ, \tau_0)} \quad (16)$$

where the variables in the parenthesis are M , the shield material; E_0 , the energy of incident gamma rays; θ_0 , the angle of incidence; and τ_0 , the slab shield thickness in mean-free-pathlengths of the incident radiation. The logarithm of $R_T(M, E_0, \theta_0, \tau_0)$ is plotted in Figs. 28-33 for the case of 1.0-, 2.5-, and 6.0-Mev gamma rays incident on iron and lead as a function of slab thickness τ_0 . Concrete ratios closely resemble the iron ratios and therefore are not plotted. It can be seen that for a given incident energy and angle, the logarithm of $R_T(M, E_0, \theta_0, \tau_0)$ vs τ_0 can be closely approximated by a straight line; that is,

$$\ln R_T(M, E_0, \theta_0, \tau_0) = -S_T(M, E_0, \theta_0)\tau_0 \quad (17)$$

and therefore

$$R_T(M, E_0, \theta_0, \tau_0) = e^{-S_T(M, E_0, \theta_0)\tau_0} \tag{18}$$

The straight lines were drawn through the point $R_T = 1.0$ and $\tau_0 = 0$ for each of the incident angles. The slopes of these lines, $S_T(M, E_0, \theta_0)$, were adjusted so as to give greater weight to the data points for thinner slabs, since these points are statistically more significant than are the data points for thicker slabs.

The data for 6.0-Mev gamma rays incident on lead slabs did not conform to the above equation for the full range of slab thicknesses and incident angles. This nonlinearity at the larger incident angles is due to the existence of a minimum in the total absorption cross section for lead at an energy less than the 6.0 Mev. Figure 34 shows how the linear range is increased when the energy of the primary gamma ray is reduced to 4.0 Mev, which is slightly above the minimum absorption at 3.4 Mev.

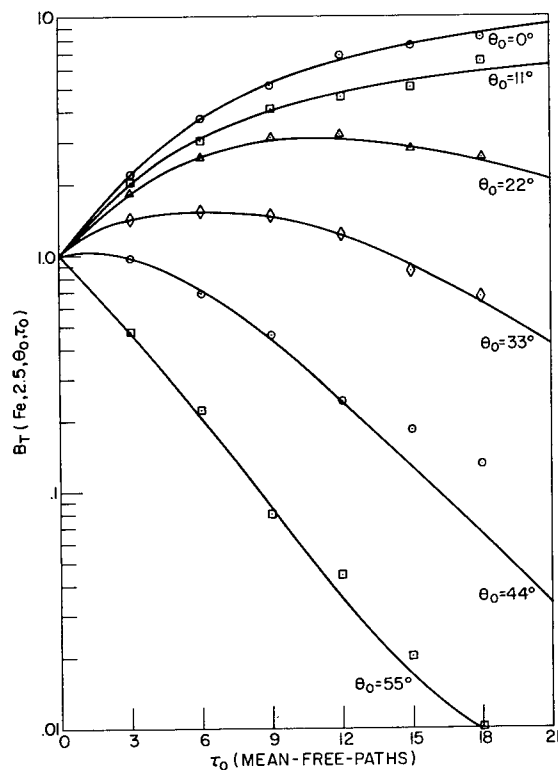


Fig. 27 - Energy penetration buildup factors, $B_T(Fe, 2.5, \theta_0, \tau_0)$, as a function of slab thickness τ_0

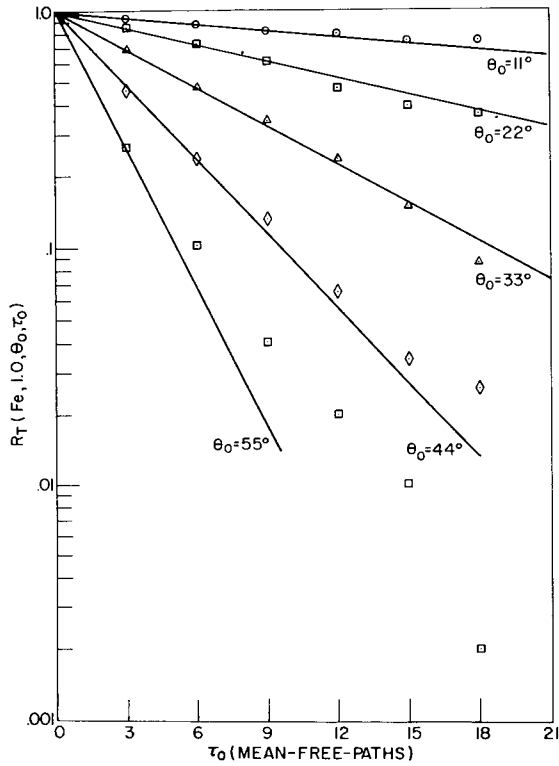


Fig. 28 - The ratio $R_T(Fe, 1.0, \theta_0, \tau_0)$ as a function of slab thickness τ_0

Fig. 29 - The ratio $R_T(Fe, 2.5, \theta_0, \tau_0)$ as a function of slab thickness τ_0

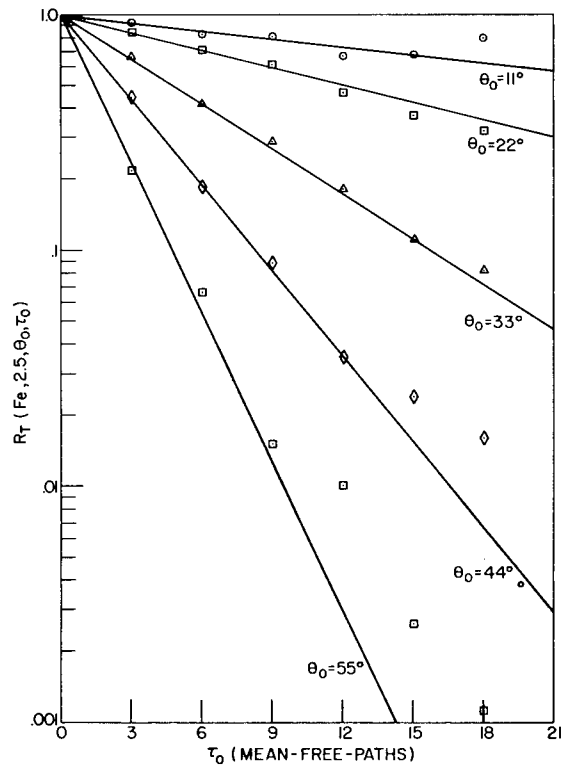


Fig. 30 - The ratio $R_T(\text{Fe}, 6.0, \theta_0, \tau_0)$ as a function of slab thickness τ_0

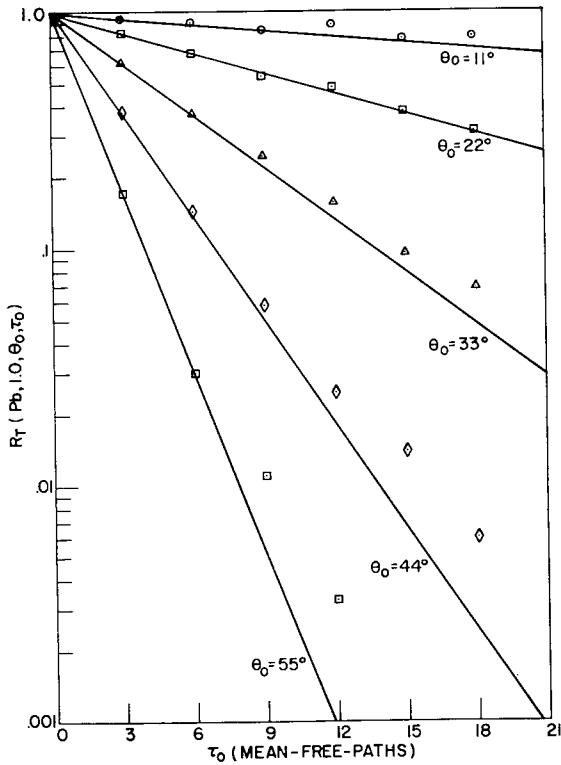
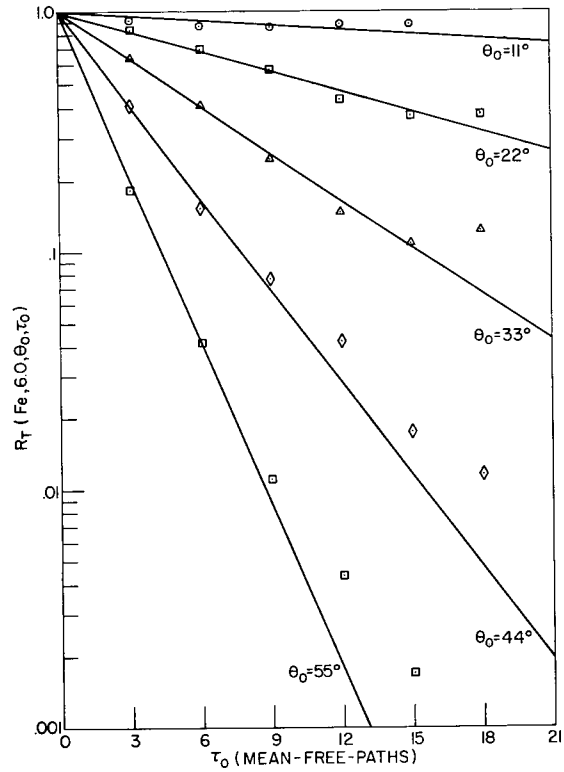


Fig. 31 - The ratio $R_T(\text{Pb}, 1.0, \theta_0, \tau_0)$ as a function of slab thickness τ_0

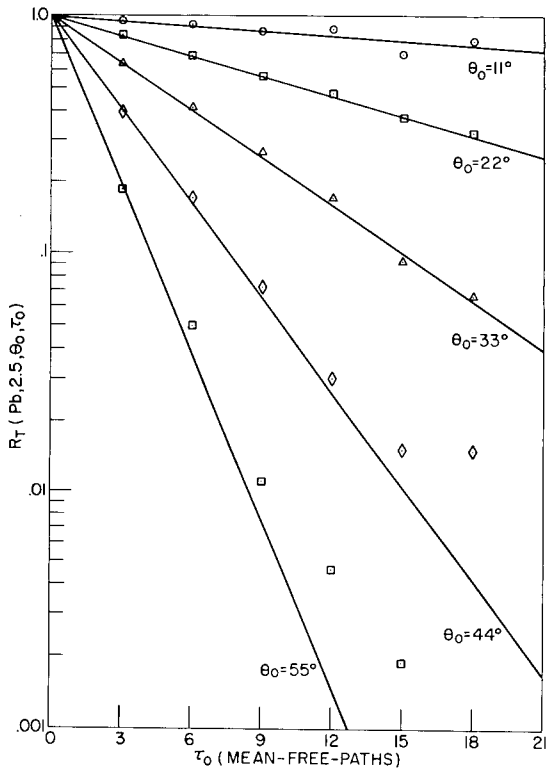


Fig. 32 - The ratio $R_T(Pb, 2.5, \theta_0, \tau_0)$ as a function of slab thickness τ_0

Fig. 33 - The ratio $R_T(Pb, 6.0, \theta_0, \tau_0)$ as a function of slab thickness τ_0

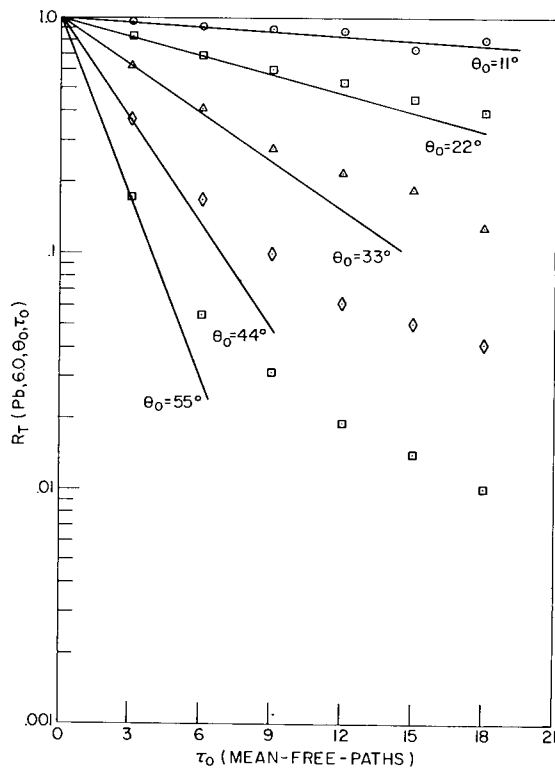
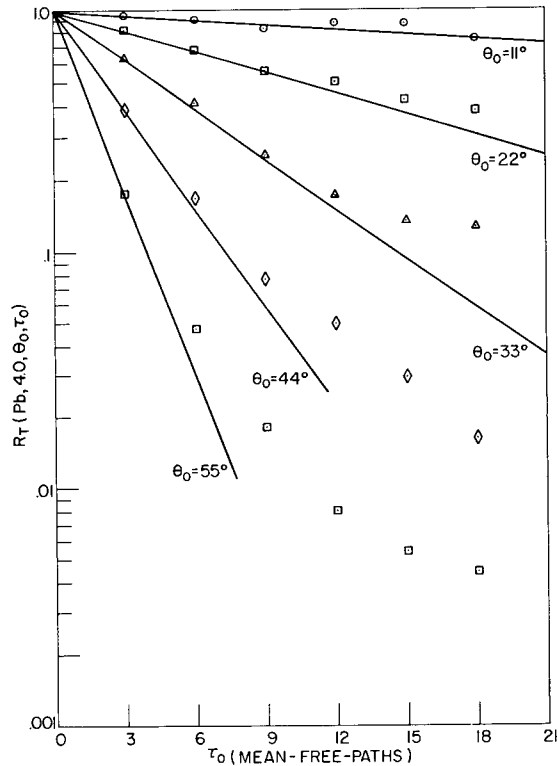


Fig. 34 - The ratio $R_T(\text{Pb}, 4.0, \theta_0, \tau_0)$ as a function of slab thickness τ_0



Thus the exponential relationship for the ratio of buildup factors given by Eq. 18 is a very good approximation so long as the energy of the incident gamma ray does not exceed the energy of minimum total absorption for the particular shield material. However, even if the energy of the incident gamma ray does exceed this limit, Eq. 18 is still satisfactory for thick shields provided the incident angle is small. Larger angles of incidence may be used in the equation only when the shield is kept sufficiently thin. The more the gamma energy exceeds that for minimum total absorption, the greater will be the restrictions on the applicability of Eq. 18. For example, these restrictions for the case of lead shields can be expressed approximately by the following inequalities:

$$\tau_0 < 18 \cos^2 \theta_0 \text{ when } E_0 = 4.0$$

and

$$\tau_0 < 12 \cos^2 \theta_0 \text{ when } E_0 = 6.0 \text{ Mev.}$$

Peebles (7) using the method of successive scatterings has calculated the energy penetration buildup factors through finite lead and iron slab shields as a function of the incident angle at a number of energies. His data was used to calculate $R_T(M, E_0, \theta_0, \tau)$ for gamma ray energies of 0.5, 1.25, 2.5, and 5.0 Mev incident at 0, 37, 53, and 66 degrees on iron and lead slabs. The plots of the logarithm of $R_T(F_e, E_0, \theta_0, \tau)$ for incident gamma-ray energies of 2.5 and 5.0 Mev on iron slabs showed the same linear relationships as our calculations showed at angles as large as 66 degrees. For 1.25-Mev gamma rays incident on iron, there is a moderately good fit to a straight line at an angle of 53 degrees and a poor fit at 66 degrees. The 0.5-Mev iron data indicate that only for an angle of 37 degrees can the plot of $\ln R_T$ vs τ_0 be approximated by a straight line. Thus Peebles' iron data indicate that there is a low energy limit for the applicability of Eq. (18). For iron this low energy limit appears to be between 0.5 and 1.0 Mev.

Peebles' 5.0-Mev lead data show the same departure from linearity as our data for 4.0 and 6.0 Mev, but this departure from linearity becomes evident sooner, that is, for thinner slabs. At 2.5 Mev linearity is restored; furthermore, this linearity is maintained down to an incident energy as low as 0.5 Mev for incident angles as large as 66 degrees.

When $S_T(M, E_0, \theta_0)$ was plotted as a function of the incident angle θ_0 for a particular gamma-ray energy and shield material, it was found that these data points could be connected by a well-behaved continuous curve. A representative example of this plot can be seen in Fig. 35 for the case of 2.5-Mev gamma rays incident on a lead shield. The values of the slopes, $S_T(\text{Pb}, 2.5, \theta_0)$, at angles of $\theta_0 = 37, 53,$ and 66 degrees were derived from Peebles' data. Plots of $S_T(M, E_0, \theta_0)$ for other gamma-ray energies and shield materials produced strikingly similar curves. The shape of these curves suggested that $S_T(M, E_0, \theta_0)$ was proportional to $[\sec(\theta_0) - 1]$. This function is indicated by the solid curve in Fig. 35. If θ_0 in the function $[\sec(\theta_0) - 1]$ is replaced by $\beta\theta_0$, the two curves can be brought into close coincidence by a proper choice of β . Thus the slopes can be expressed as

$$S_T(M, E_0, \theta_0) = \sec(\beta\theta_0) - 1 \quad (19)$$

and consequently the expression for ratio of buildup factors (Eq. 18) can be simply written:

$$R_T(M, E_0, \theta_0, \tau_0) = e^{-[\sec(\beta\theta_0) - 1]\tau_0} \quad (20)$$

Whether Eq. (19) is a satisfactory expression for the slopes can be easily demonstrated by rewriting it in the following form:

$$\beta\theta_0 = \sec^{-1}[1 + S_T(M, E_0, \theta_0)]. \quad (21)$$

This equation shows that if the angle $\sec^{-1}[1 + S_T(M, E_0, \theta_0)]$ is plotted as a function of θ_0 , these points should lie on a straight line which goes through the origin and the slope of this line is just equal to the parameter β . Plots of this function for 2.5-Mev gamma rays incident on three different materials (iron, concrete, and lead) are shown in Figs. 36-38. The values of $\sec^{-1}[1 + S_T(M, E_0, \theta_0)]$ derived from Peebles' 2.5-Mev gamma-ray buildup factors in iron and lead are also included. With the exception of the 11-degree point for iron, all the data points for these three materials were in excellent agreement with Eq. (21), not only for 2.5-Mev gamma rays but also for 1.0-Mev and 6.0-Mev gamma rays. The parameter β derived from these plots varied between 0.83 and 0.93 for gamma-ray energies between 1.0 and 6.0 Mev. The values of $\sec^{-1}[1 + S_T(M, E_0, \theta_0)]$ for the various energy gamma rays incident at 11 degrees on both iron and concrete were not consistent with the data for larger incident angles. However, this anomalous behavior at 11 degrees does not appreciably affect the adequacy of representing the ratio of buildup factors by Eq. (20). That is, the values of $R_T(M, E_0, \theta_0 = 11^\circ, \tau_0)$ calculated from Eq. (20) were within 10 or 15 percent of the Monte Carlo derived values of this ratio, even for τ_0 as large as 18 mean-free-pathlengths.

An identical analysis of the ratio of the dose-rate buildup factors revealed that these buildup factors were also related by the same exponential function as derived for the energy penetration buildup factors. The evaluation of the parameter β for the dose-rate buildup factors showed that they were slightly larger than the corresponding energy penetration parameter in iron, concrete, and water, whereas in lead the two parameters were commensurate. In fact, in lead we found that

$$\frac{B_R(\text{Pb}, E_0, \theta_0, \tau_0)}{B_R(\text{Pb}, E_0, 0^\circ, \tau_0)} = \frac{B_T(\text{Pb}, E_0, \theta_0, \tau_0)}{B_T(\text{Pb}, E_0, 0^\circ, \tau_0)} \quad (22)$$

for the complete range of θ_0 and τ_0 even when the incident energy exceeded the energy of minimum total absorption, which is a condition on the applicability of Eq. (20) for lead.

Fig. 35 - $S_T(\text{Pb}, 2.5, \theta_0)$ as a function of incident angle θ_0

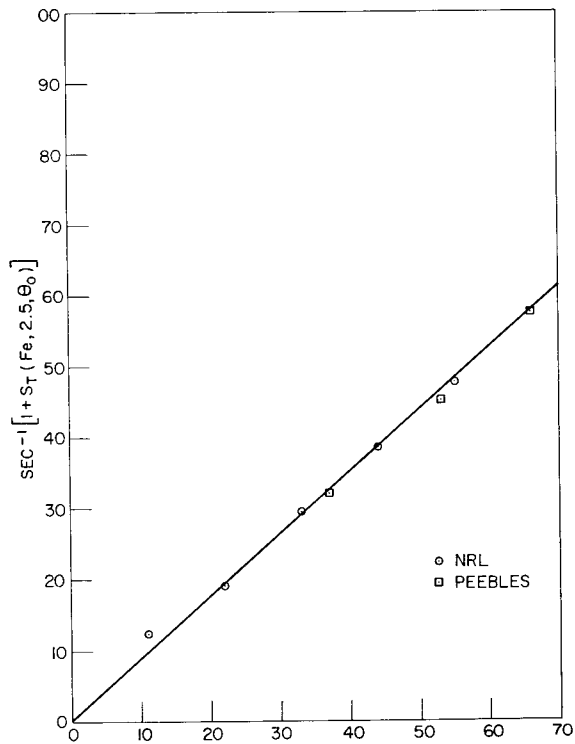
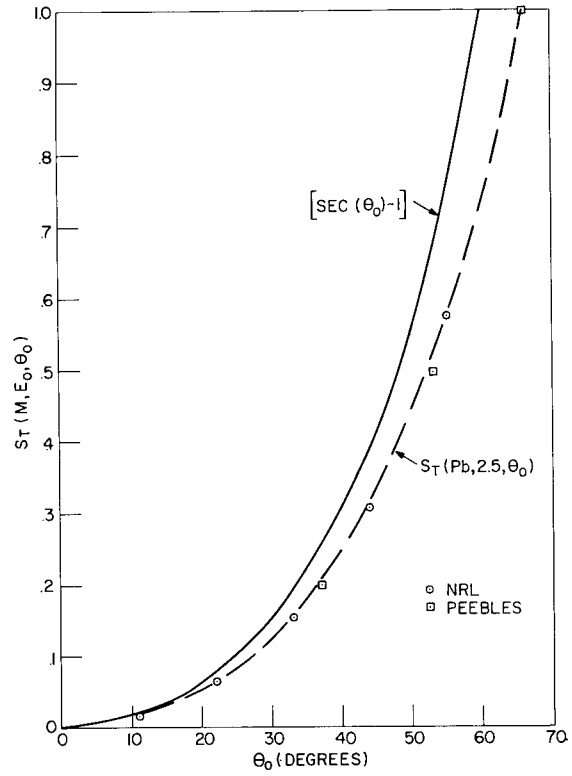


Fig. 36 - $\text{SEC}^{-1}[1 + S_T(\text{Fe}, 2.5, \theta_0)]$ as a function of incident angle θ_0

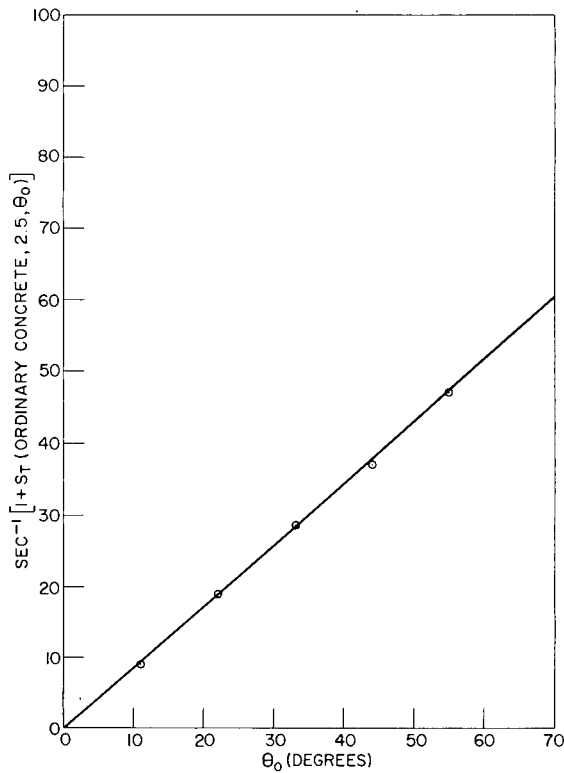


Fig. 37 - $\text{Sec}^{-1} [1 + S_T(\text{Concrete, 2.5, } \theta_0)]$ as a function of incident angle θ_0

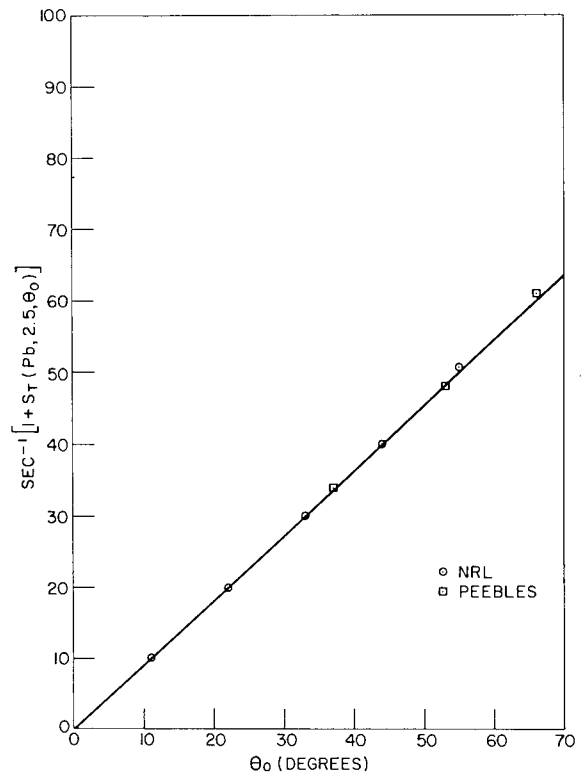


Fig. 38 - $\text{Sec}^{-1} [1 + S_T(\text{Pb, 2.5, } \theta_0)]$ as a function of incident angle θ_0

We did not calculate energy flux buildup factors, but it was possible to derive these from our tabulated dose-rate spectra. The ratio of the energy flux buildup factors for a few different conditions demonstrated that these buildup factors were also related by the same exponential function as given by Eq. (20). Furthermore, it was found that the parameters for energy flux were commensurate with the parameters for dose-rate, and therefore

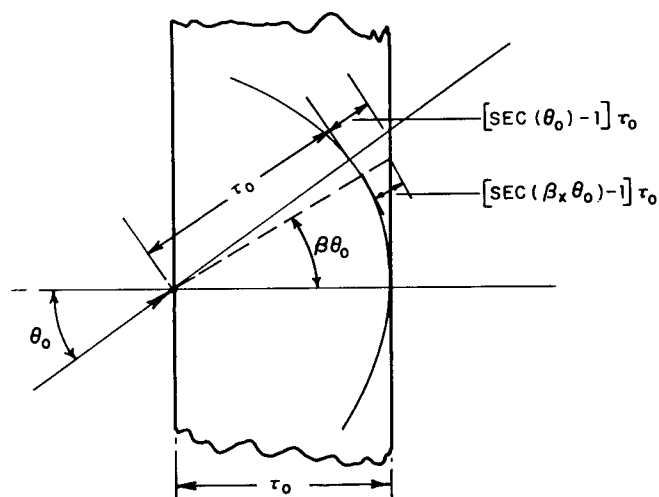
$$\frac{B_E(M, E_0, \theta_0, \tau_0)}{B_E(M, E_0, 0^\circ, \tau_0)} = \frac{B_R(M, E_0, \theta_0, \tau_0)}{B_R(M, E_0, 0^\circ, \tau_0)} \quad (23)$$

Actually this relationship can be derived because dose-rate is equal to energy flux times the energy absorption coefficient for gamma rays in air, and this coefficient is practically constant over a significant range of gamma-ray energies.

Expressing Eq. (20) in terms of buildup factors we have the following simple relationship

$$B_X(M, E_0, \theta_0, \tau_0) = B_X(M, E_0, 0^\circ, \tau_0) e^{-[\sec \beta_X \theta_0 - 1] \tau_0} \quad (24)$$

where the subscript X designates the type of buildup factor or buildup quantity. The parameter β is used with a subscript because of its slight dependence on the buildup quantity in most materials. The physical significance of the exponent $[\sec(\beta_X \theta_0) - 1] \tau_0$ can be seen by referring to the following illustration, which depicts the penetration of obliquely incident gamma rays through a slab τ_0 mean-free-pathlengths thick.



If the parameter β_X were equal to 1.0 then the exponent $[\sec(\theta_0) - 1] \tau_0$ would be just equal to the difference between the slant and the perpendicular penetration distances through a slab τ_0 mean-free-pathlengths thick. The fact that β_X is actually less than 1.0 indicates that obliquely incident gamma rays are being bent or refracted toward the normal direction. This refractive effect is to be expected because those gamma rays which are scattered toward the normal direction have shorter pathlengths and thus have greater probability of emergence than do those scattered away from the normal direction. Consequently, β_X is referred as the "X quantity refraction parameter."

The variation of the energy penetration refraction parameter β_T as well as the dose-rate refraction parameters β_R , is plotted against the incident gamma-ray energy in Figs. 39-41 for iron, concrete, and lead. There are only three points for concrete, so the energy dependence of β_T and β_R is somewhat uncertain. However, this dependence does not differ appreciably from the corresponding iron parameters for gamma-ray energies less than 4.0 Mev. This similarity in the refraction parameters is to be expected because the predominant gamma-ray interactions in this range of energies for both these materials are Compton scatterings. Concrete is predominantly a Compton scatterer even at 6.0 Mev, and thus the refraction parameters for concrete are applicable to all shielding materials in which the Compton type of gamma-ray interactions predominate. This conclusion was subsequently confirmed by the evaluation of the refraction parameters for 6.0-Mev gamma rays in water, which is an even better Compton scatterer than concrete.

The refraction parameters for these Compton materials increase with energy because of the increased peaking in the primary direction of the Klein-Nishina differential cross section function as the energy increases. Consequently, an obliquely incident beam of radiation will be refracted less at the higher energies.

The reason the refraction parameters in lead are larger than the refraction parameters for Compton type of materials at the lower energies is due to the increasing importance in lead of photoelectric absorption at energies below 2.5 Mev. The high probability of photoelectric absorption at these lower energies will rapidly remove those gamma rays that deviate

appreciable from the incident direction. Thus refraction is curtailed because those gamma rays which survive a single or multiple scattering are largely confined to the primary direction.

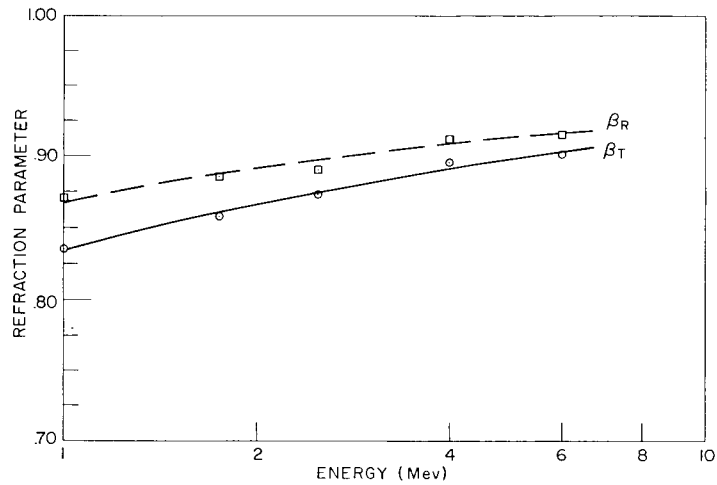


Fig. 39 - Energy penetration and dose-rate refraction parameters for iron as a function of gamma-ray energy in Mev

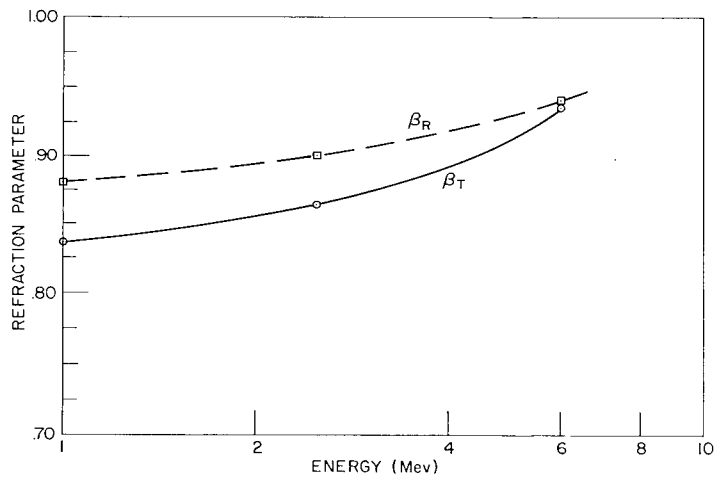


Fig. 40 - Energy penetration and dose-rate refraction parameters for concrete as a function of gamma-ray energy in Mev

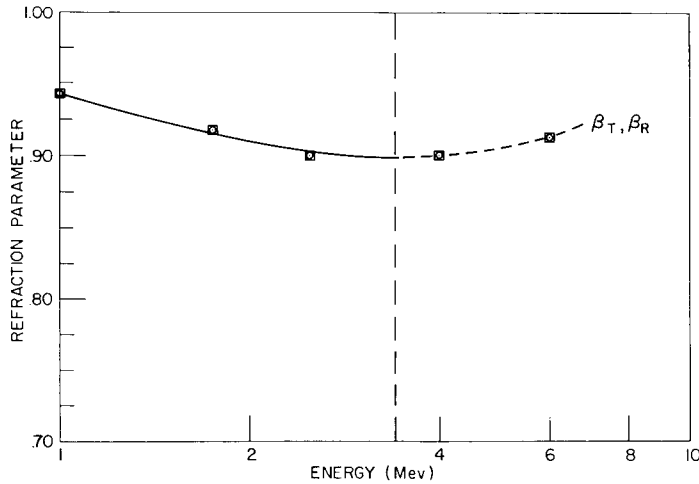


Fig. 41 - Energy penetration and dose-rate refraction parameters for lead as a function of gamma-ray energy in Mev

CONCLUSION

Solutions to the gamma-ray transport equation for slab shields were obtained by Monte Carlo methods using the exponential transformation type of biasing. The energy penetration and the dose-rate probabilities through slab shields of lead, iron, ordinary concrete, and water were calculated for a plane, monodirectional source of gamma rays incident on these slabs at various angles. The energy penetration and dose-rate buildup factors derived from these calculations were in good agreement with the corresponding buildup factors derived by other computational methods.

A simple relationship between the buildup factors of obliquely and normally incident gamma rays has been graphically derived. This relationship can be expressed in the following manner:

$$B_X(M, E_0, \theta_0, \tau_0) = B_X(M, E_0, 0^\circ, \tau_0) e^{-(\sec \beta_X \theta_0 - 1)\tau_0}$$

where $B_X(M, E_0, \theta_0, \tau_0)$ is the buildup factor of the quantity X, when gamma rays of energy E_0 are incident at θ_0 degrees on slab shields τ_0 mean-free-pathlengths thick of shielding material M; and $B_X(M, E_0, 0^\circ, \tau_0)$ is the corresponding buildup factor of normally incident gamma rays.

The incident angle coefficient β_X , which is referred to as the "X quantity refraction parameter" is a slowly varying function of the energy of the incident gamma ray for a given shield material. The values of three types of refraction parameters (energy, dose-rate, and energy flux) were all within the limits

$$0.80 < \beta_X < 0.95$$

for gamma-ray energies from 1.0 to 6.0 Mev in all of the shielding materials under investigation.

REFERENCES

1. Beach, L.A., Theus, R.B., Plawchan, J.D., and Faust, W.R., "Stochastic Estimates of X-Ray Spectral Intensities For Shallow and Deep Penetrations," NRL Report 4412, Aug. 3, 1954
2. Kahn, H., *Nucleonics* 6(No. 5):27 (1950); 6(No. 6):60 (1950)
3. Beach, L.A., Theus, R.B., Shapiro, P., O'Rourke, R.C., Faust, W.R., and Lepson, B., "Comparison of Solutions to the One-Velocity Neutron Transport Problem," NRL Report 5052, Dec. 1957
4. Spencer, L.V., and Fano, U., *Phys. Rev.* 81:464L (1951) and *J. Research, Nat. Bur. Standards* 46:446 (1951)
5. Grodstein, G. White, "X-Ray Attenuation Coefficients from 10 kev to 100 Mev," NBS Circular 583 Apr. 30, 1957
6. Davisson, C.M., private communication
7. Peebles, G.H., "Gamma-Ray Transmission Through Finite Slabs," The Rand Corp., R-240, Dec. 1, 1952
8. Goldstein, H., and Wilkins, J.E., Jr., "Calculation of the Penetration of Gamma Rays," AEC, NYO 3075, June 30, 1954
9. Berger, M.G., and Doggett, J., "Reflection and Transmission of Gamma Radiation by Barriers: Semianalytic Monte Carlo Calculation," *J. Research, Nat. Bur. Standards* 56:89 (1956)
10. Davisson, C.M., and Beach, L.A., "Gamma-Ray Albedos of Iron," *NRL on Nuclear Science and Technology*, pp. 43-58, Oct - Dec. 1959
11. Davisson, C.M., private communication